Fixed Wing UAV Design

Final Project Report

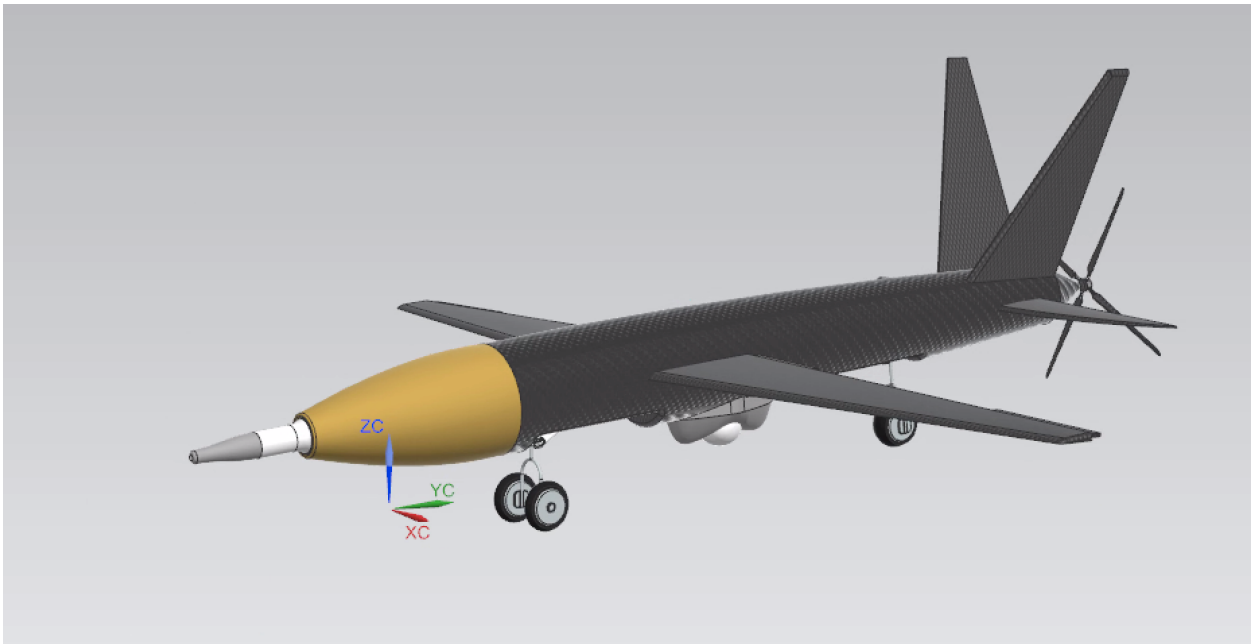

Created by:
Parth Patel

Dr. Denis Dorozhkin

ME 4042 (Advanced CAD & CAE)

Georgia Tech College of Engineering
George W. Woodruff School of Mechanical Engineering

Table of Contents

Motivation

The development of small, mission-ready unmanned aerial vehicles has accelerated in the last decade, and the gap between large strategic platforms and disposable tactical systems has widened. This project takes its cues from both ends of that gap. The MQ-9 Reaper sets the operational profile we wanted to study at a smaller scale, including long endurance, fixed-wing efficiency, and a payload bay that can carry sensors instead of just propulsion hardware. The Anduril ALTIUS family informs the size class and the rapid-deployment philosophy, where a UAV is treated as a consumable that needs to be cheap enough to scale and rugged enough to be useful before it is lost.

The drone modeled in this report is purpose built as a small fixed-wing platform aimed at counter-UAS defense. The design philosophy centers on rapid manufacturing and the integration of commercially available components. The fuselage uses lofted carbon fiber surfaces over a payload bay, the wings are tapered carbon fiber with movable flaps, and the propulsion is a four-blade rear-mounted propeller driven through a hub assembly. Landing gear, sensor mount, and pitot tube are all separate parts so they can be revised or swapped without touching the airframe. The goal is a vehicle that can be CAD-iterated, FEA-validated, and built by a small team in a tactical environment.

Introduction

This report documents the design and analysis of a small fixed-wing UAV from CAD modeling through structural validation. The drone was modeled in Siemens NX as a complete assembly of around twenty separate parts mated together with constraints, then critical components were carried through finite element analysis to check stress and deflection under representative load cases.

The modeling effort uses both surface and solid techniques depending on the part. Lofted Through Curves and swept profiles drive the aerodynamic surfaces, and solid feature trees handle the mechanical hardware. FEA was performed on the wings under a distributed lift pressure and on the front landing gear U-link under a tension load. Hand calculations based on cantilever beam theory are used to validate the FEA, and a final crash-load attempt on the full assembly is included to document what worked and what did not. Future work is discussed in terms of theoretical improvements to the landing gear suspension and the wing flap actuation.

Modeling

All parts were created in Siemens NX. The full assembly file ME4042_UAV_FULL_ASSM_FINAL holds 43 components and 31 assembly constraints, including Align, Center, Touch, Concentric, Parallel, Distance, Fix, and Align/Lock. The fuselage is fixed at the world origin and every other part is mated against it, which makes the body the parent of the assembly tree. The sections below describe how each major component was built and how the design decisions in each part feed into the assembly.

Main Body

The main body was created using a series of three circular profiles with a Through Curves surface generated between them. The circular profiles created a consistent cross section in the middle of the body where the wings would be attached, and a tapered section toward the back where the rear propeller would be attached. This tapered profile allowed for proper aerodynamics, and continuity was carried throughout the body with the singular surface created. To close the front and back sections of the body, a Bounded Plane feature was used to create surfaces along those planes. The entire body was then sewn together to create a full solid body. Figure 1 shows the solid body with the circular loft profiles highlighted.

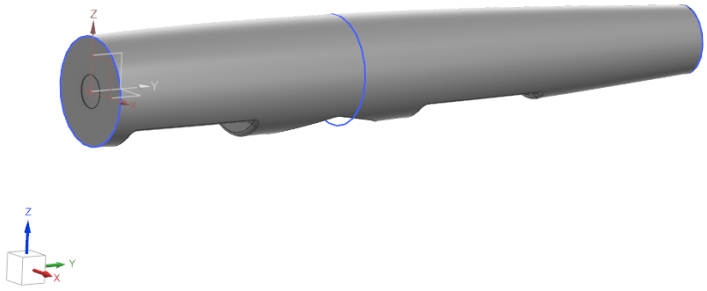

Figure 1: *Main body as a solid body with circular loft profiles highlighted.*

Once the solid body of the drone was created, mating features for external components were added to drive the full assembly. This involved sketching profiles along a plane below the bottom of the main body and extruding into the solid body, using the Subtract feature to remove material where particular components like the landing gear and camera connect. Edge Blends were used on all sharp edges that the subtraction created to ensure smoother continuity between faces. Figure 2 shows the resulting recesses on the underside.

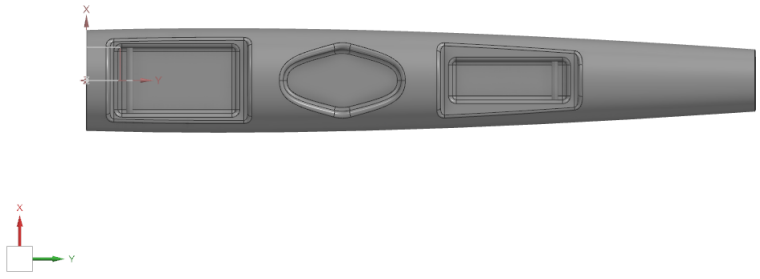

Figure 2: *Mating features on bottom of main body.*

Nosecone

Creation of the solid body for the nosecone followed a similar process to the main body. Three circular profiles were created on three spaced-out planes and a Through Curves function was used to create a continuous surface between them. The first profile sets the diameter where the nose meets the fuselage, and the third profile pulls the surface forward to a smaller circle near the tip.

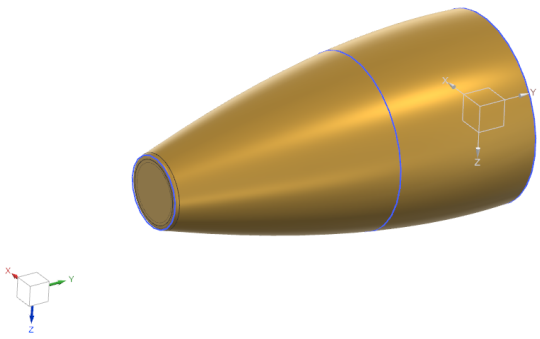

Figure 3: *Nosecone modeling with through curves profiles highlighted.*

A key design intent for the nosecone was to keep a hollow interior so that payloads could be stored inside before the drone enters flight. To do this, a second surface was generated using the same circular profiles but scaled down so a wall thickness of 5 mm was achieved. Bounded Planes were created between the inner and outer surfaces to fully close out the geometry, and a Sew command was used to make the nosecone a solid body. A second circular profile was generated on the tip for the remaining opening and Extruded into the body to create the final geometry. Edge Blends were applied to the surface joining edges for better continuity. Figure 4 shows the resulting hollow interior.

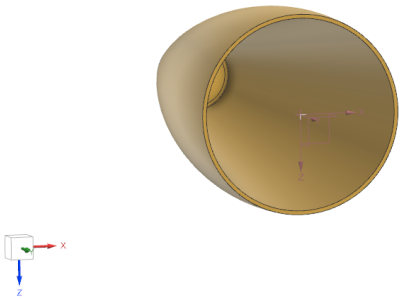

Figure 4: *Hollow interior of nosecone using sewn surfaces.*

To improve the aerodynamics of the tip, a Pitot Tube component was generated to mate onto the front flat surface of the nose. The Pitot Tube was generated using a cross-section profile that was Revolved around the centerline. The profile uses two Cubic Bezier Splines drawn in a single plane: one taper at the front near the tube opening and another at the back where it mates onto the nosecone. The Revolve feature created the solid body, and Edge Blends cleaned up the surface joins.

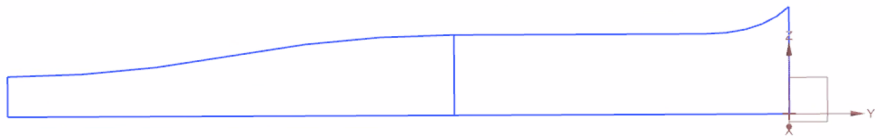

Figure 5: *Cubic Bezier spline sketches used for pitot tube modeling.*

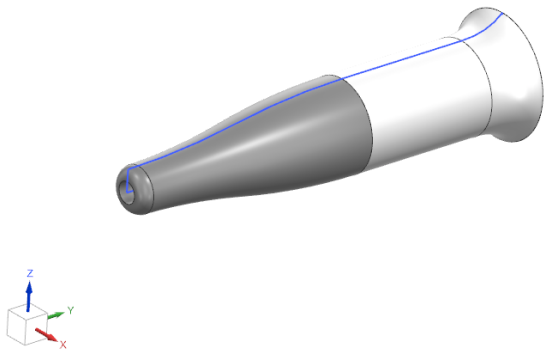

Figure 6: *Solid body of pitot tube generated from cubic Bezier splines.*

Wings

The side wings were the most surface-heavy part in the model and went through the largest revision since the previous report. The original wing was a single lofted body with no movable surface. The current part, ME4042_UAV_SIDE_WINGS, is built from a Sketch on the root datum plane that defines the airfoil profile, two Splines that drive the leading and trailing edges along the span, and three Fill Surface features that close out the pressure side, the suction side, and the wing tip. A second sketch defines the cutout where the flap sits. After the surfaces are sewn into a solid body, seven Edge Blend features round the leading edge, the trailing edge, the tip, and the corners at the root. The taper from a 0.15 m chord at the root to a 0.05 m chord at the tip is set by the spline endpoints rather than by separate sketches, which keeps the wing easy to rescale.

A flap was added as a separate part, ME4042_UAV_flaps, mated to the inboard trailing edge of the side wing. The flap was modeled by Extruding a sketched profile into a thin block, applying four Edge Blends along the leading and trailing corners to round the profile, and finishing with a Move Face on the inboard end so the flap sits flush against the cutout in the wing. Modeling the flap as a separate body lets the assembly control the flap deflection through a single mate, which means the same wing geometry can be reused for cruise, takeoff, and landing configurations without rebuilding the wing solid. The same approach was used for the right wing through ME4042_UAV_flaps_2, mirrored across the centerline.

Carbon fiber was selected as the wing material on a strength-to-weight basis. The visible weave appearance in the assembly views comes from a custom material applied in NX rather than from a true laminate definition, which is the simplification carried through to the FEA section. Figures 7 through 9 show the side wing with the flap installed.

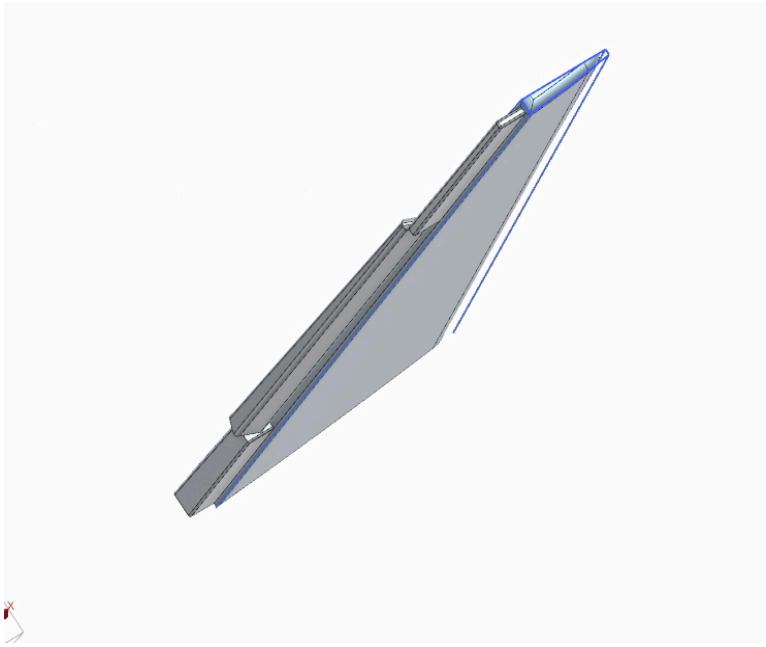

Figure 7: *Side wing diagonal view with flap installed along the trailing edge.*

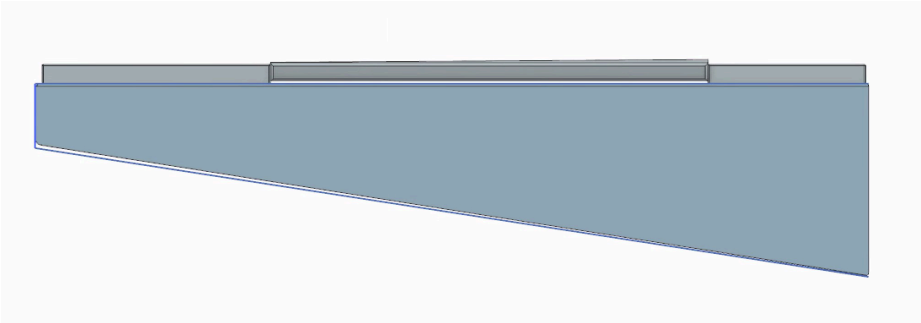

Figure 8: *Top view of side wing with flap profile visible at the trailing edge.*

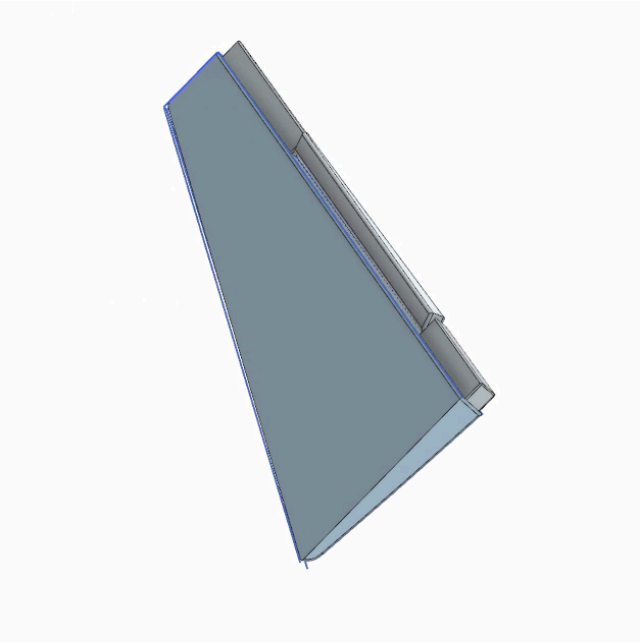

Figure 9: *Close-up of wing root showing flap as a separate body mated to the wing.*

Landing Gear

The landing gear for the front and rear of the body were modeled with a similar process. The wheels were created using three circular profiles with a Through Curves feature used to generate a surface between them. Solid modeling features on the outside formed the hubcaps. A cylindrical mating feature in the middle was added with a Subtract feature so the wheel can mate to the linkage that connects to the body.

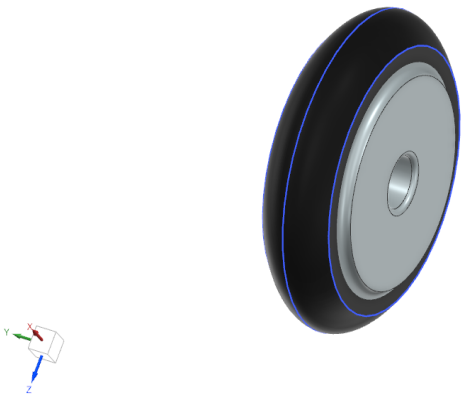

Figure 10: *Solid body of wheel with circular profiles displayed.*

The linkage connecting the wheels to the main body was created in the shape of a U-bar, using a swept profile of a circle over a U-shaped path. A mating feature at the top allows the linkage to mate to the body and rotate the wheel during deployment. Axles for the wheels to sit on were added at the bottom of the linkage using solid modeling. Two axles were added for the front landing gear and one for the rear. Edge Blends were added to all sharp edges to smooth continuity between faces.

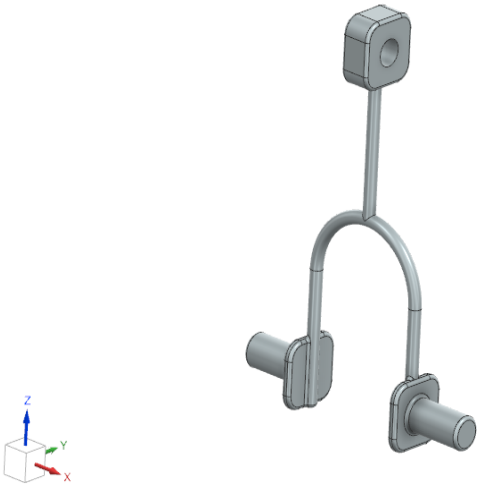

Figure 11: *Front landing gear linkage.*

Figure 12: *Rear landing gear linkage.*

A hook linkage was created to connect the swept section of the U-link with the hydraulic actuator. This involved a solid modeling process with two circular profiles connected in orthogonal orientations. The hook can slide along the swept profile of the linkage as the actuator extends, which produces the rotation of the wheel during the landing sequence.

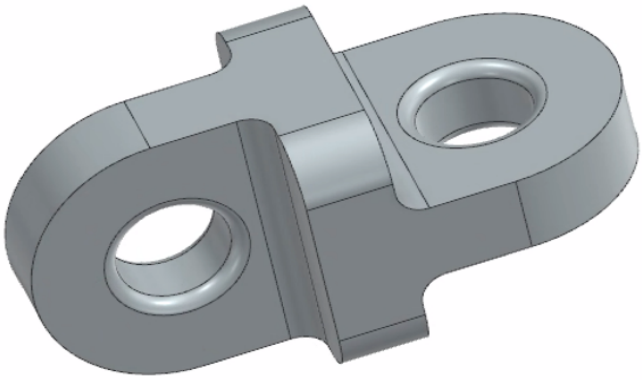

Figure 13: *Hook linkage for connecting wheel linkage to actuator.*

The actuators represent hydraulics for the opening and closing sequence of the landing gear. They were created using concentric cylindrical profiles, with a protruding feature on the end of the inner actuator that stops the travel at maximum extension. Pin connection points were added at the front of the inner actuator to connect to the hook on the wheel linkage and at the back of the outer actuator to connect to the body of the UAV. Two sets were created separately for the front and rear landing gear because of the different lengths and wheel locations, which keeps the parts from overlapping. In the full assembly these parts automatically extend and retract as the wheel linkage rotates between the open and closed positions.

Figure 14: *Hydraulic actuator outer cylinder with pin connection.*

Figure 15: *Hydraulic actuator inner cylinder.*

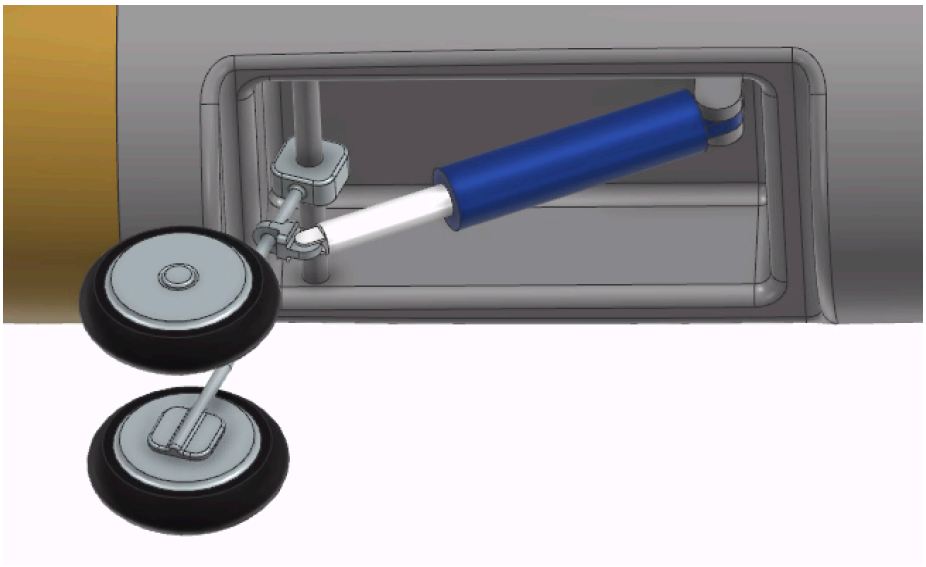

Figure 16: *Assembly orientation of front landing gear in open position.*

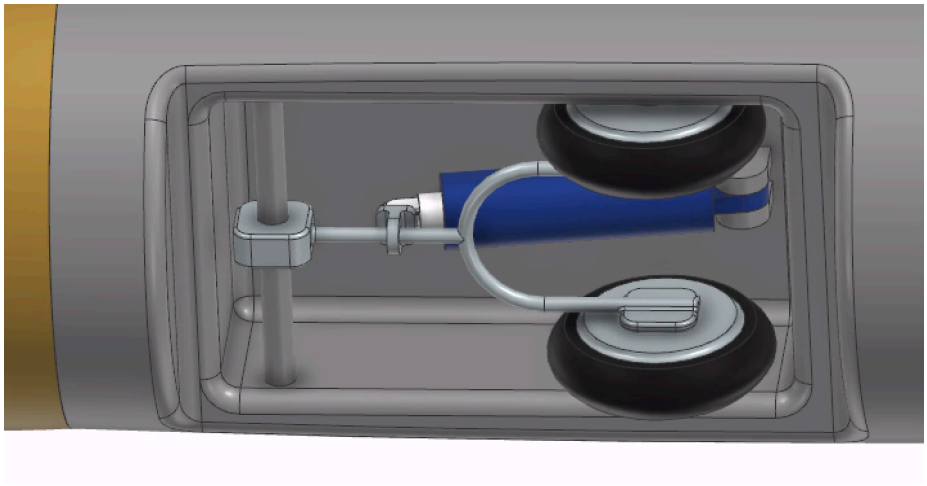

Figure 17: *Assembly orientation of front landing gear in closed position.*

Propeller

The propulsion is a four-blade rear-mounted propeller built up from individual parts and brought together in ME4042_UAV_Propeller_assembly. The hub is a Revolved cylindrical body that holds the four blade roots and provides the rotation axis for the assembly. A rounded rear cap, also revolved, sits behind the hub and serves as the fairing where the propeller meets the tail of the fuselage. Both bodies were edge blended where they meet so the surface continuity is maintained in renders.

Each blade was modeled as its own part. The core blade geometry came from a swept surface profile along a defined path, which sets the airfoil shape and the twist along the span. The solid body was built up by Extruding from fixed datum planes and sketches and then refined with multiple Face Blend operations to create the smooth curvature needed for airflow. A Scale Body feature at the end sized the blade to match the rotor hub specifications without rebuilding the sketches. Each blade is its own part file (ME4042_UAV_blade_1, blade_2, propeller3, propeller4) so individual blades can be swapped if the design moves to different airfoils.

In the propeller assembly, the four blades are mated to the hub through Concentric and Distance constraints around the rotation axis at 90 degrees apart. The whole propeller assembly is then mated to the rear of the fuselage so it can rotate as a rigid body relative to the airframe. The mate set was kept loose enough that the propeller can be hidden or replaced without breaking the constraints elsewhere in the assembly.

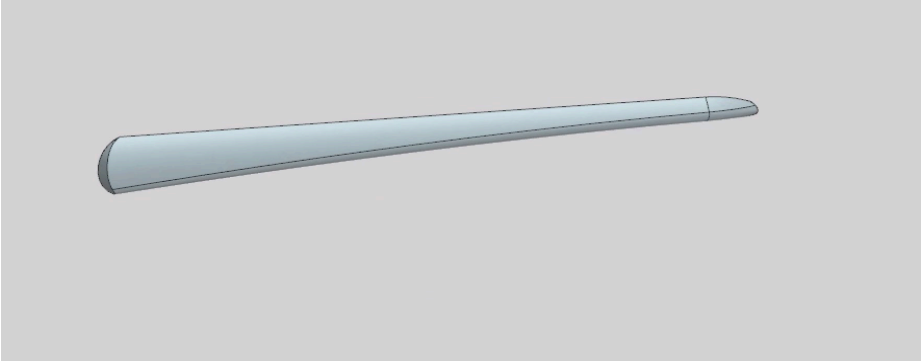

Figure 18: *Single propeller blade with swept airfoil and rounded tip.*

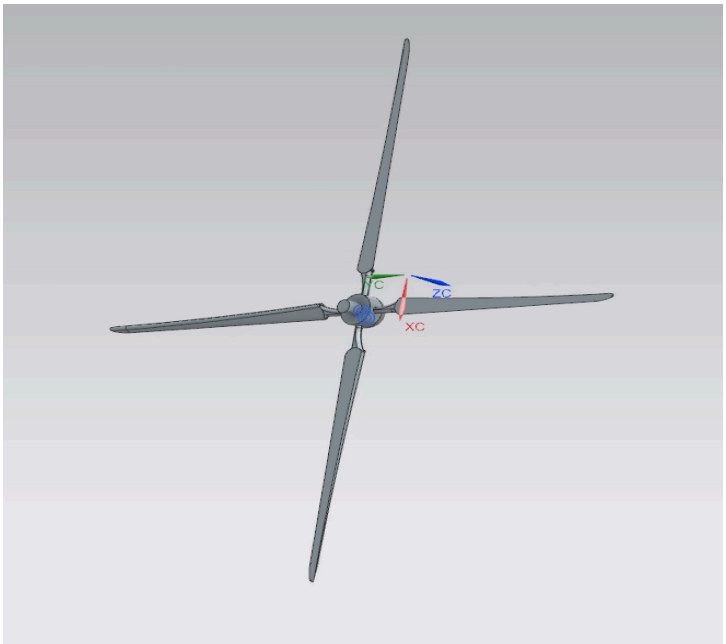

Figure 19: *Full four-blade propeller assembly.*

Camera Mount

The camera mount sits on the underside of the fuselage and was modeled as a hybrid of solid and surface features. A Cubic Bezier Spline was sketched on the bottom face and mirrored across four quadrants, then Extruded upward so the mating block fits the cavity in the main body. The aerodynamic taper on the front side comes from the Bezier curve at the leading edge of that sketch.

The upper saddle that holds the camera was created on the cross-sectional plane using a Through Points Spline, symmetric about the centerline. Combined with the bottom edge sketch and the Through Curves tool, this generated a continuous surface across the profiles with a recessed area at the top where the camera could be placed. The sheet body was then sewn into the solid body of the base. Figures 20 through 23 show the curves used and the resulting body.

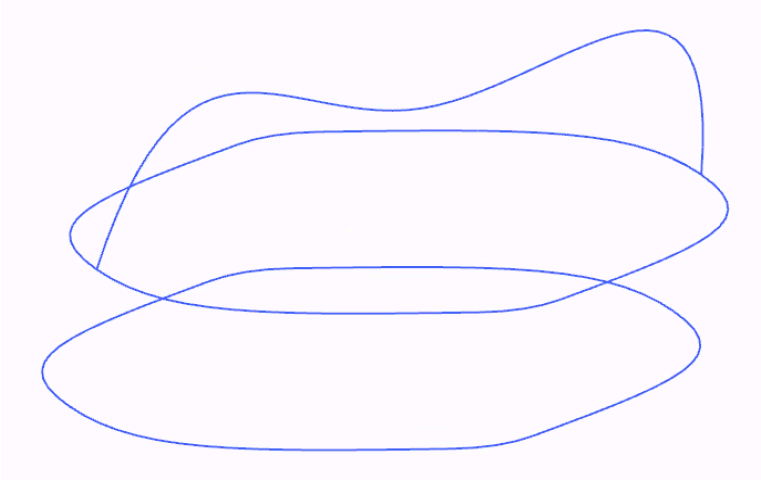

Figure 20: *Curves used for the faces of the camera mount.*

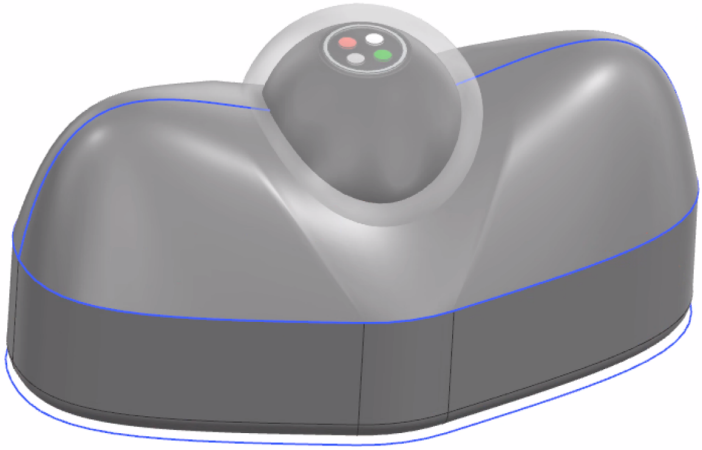

Figure 21: *Splines used for camera mount solid body geometry.*

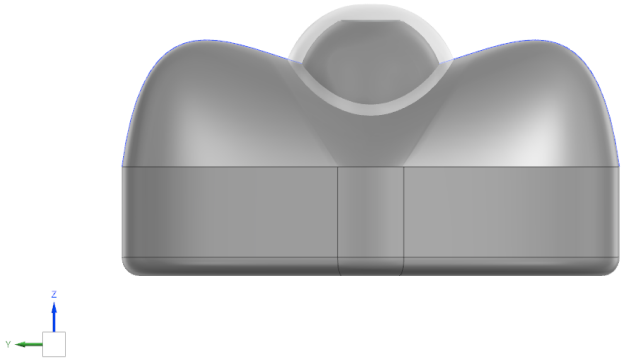

Figure 22: *Side view of camera and camera mount.*

Figure 23: *Top view of camera and camera mount.*

The camera was generated over the solid body using two Revolve features with circular cross sections to create two concentric spheres. The inner sphere was given a black appearance to match the body of a camera, and the outer sphere a white color with transparency to represent the lens. A slice was cut out of the top of the camera sphere and recording and camera symbols were added to make the part read as a sensor in renders.

Full Assembly

All parts come together in ME4042_UAV_FULL_ASSM_FINAL. The fuselage is held with a Fix constraint at the world origin, and the rest of the model is mated against it through 31 assembly constraints. The nosecone uses a Touch and an Align to seat against the front of the body, and the pitot tube concentrically mates onto the front face of the nosecone. The side wings, rear wings, and rear stabilizers are each fixed to their respective cutouts on the fuselage. The front and rear wheel sub-assemblies (each a separate ASSM file with three or four constraints inside) are mated through the hook and actuator parts so that the gear can be displayed open or retracted. The propeller assembly is mated to the rear of the fuselage with a Concentric and an Align/Lock so the four blades stay perpendicular to the rotation axis.

The four standard views of the final assembly are shown below. The fuselage and wings render as carbon fiber, the nosecone as the gold protective coating used on radomes, and the pitot tube as bare aluminum. The camera, actuators, and hub hardware are displayed in their as-modeled appearances rather than colored to match the rest of the airframe.

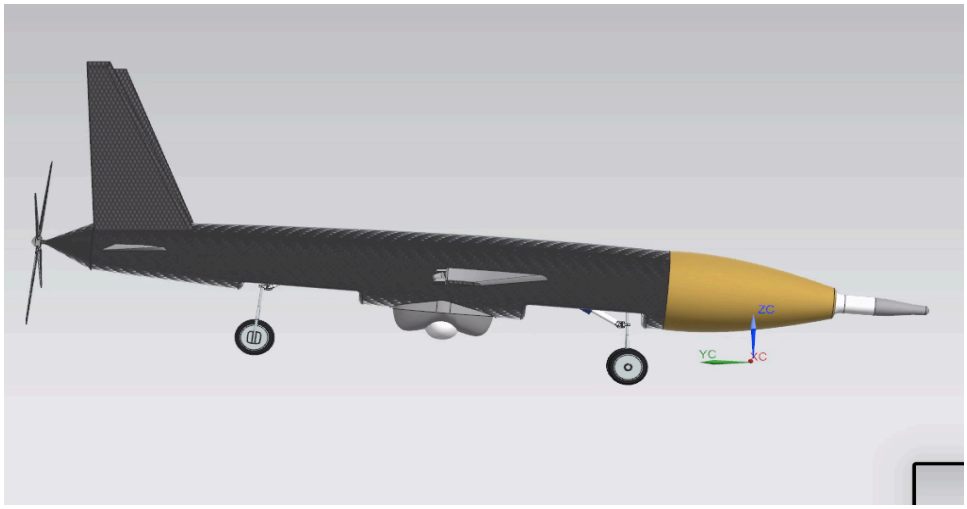

Figure 24: *Full assembly side view.*

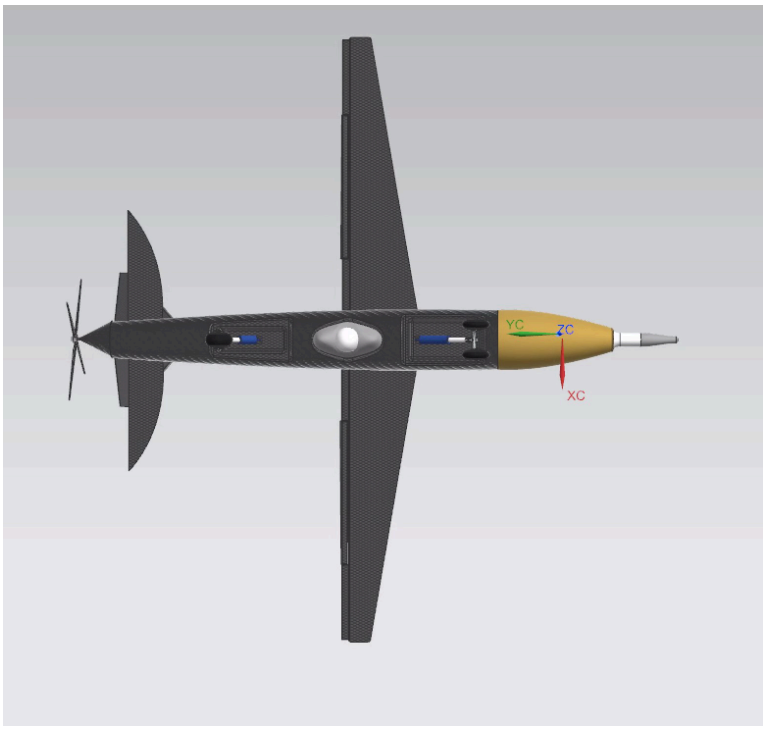

Figure 25: *Full assembly top view with payload bay covers visible.*

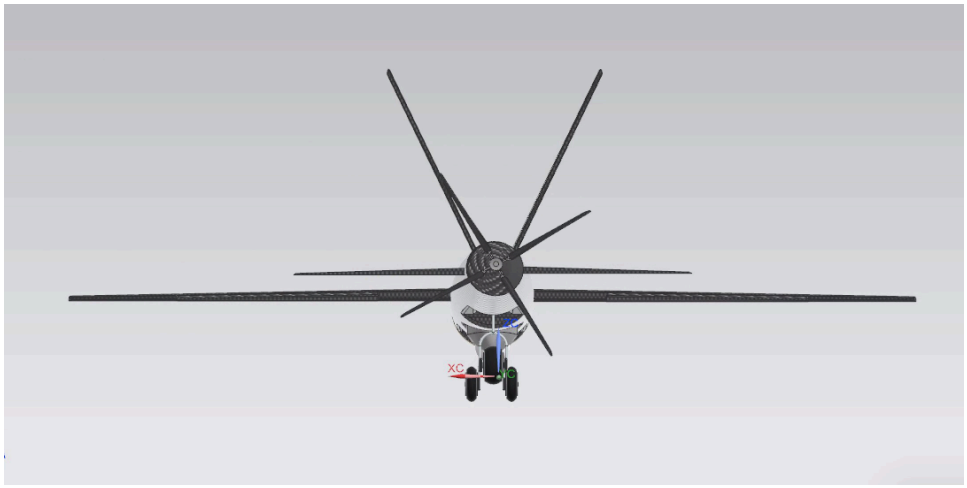

Figure 26: *Full assembly front view showing the wing span and propeller diameter.*

Figure 27: *Full assembly perspective view.*

Finite Element Analysis (FEA)

The structural performance of the UAV was evaluated using finite element analysis to assess the ability of critical components to withstand operational loading. The wings and the front landing gear U-link were selected for detailed analysis because they carry the largest aerodynamic and impact loads. The wings see distributed lift pressure that drives bending stress at the root, which is the location that sets the wing material decision. The U-link sees a tension load every time the gear takes weight on landing, which is the location that sets the gear material decision. A third FEA was attempted on the full assembly under a simulated nose impact and is documented for completeness.

Wings

FEA was conducted on the side wing of the UAV to evaluate the structural response under flight loading. The analysis predicts the stress distribution and deflection across three different materials and two different loading scenarios.

Mesh Generation and Refinement

A 3D tetrahedral mesh was generated over the wing volume using an element size of 4 mm along the full length. Mesh refinement was applied at the wing root, where the highest stress was expected from cantilever bending. Convergence was checked, and a finer element size of 1 mm was used in the root region. Anything smaller increased compute time without changing the resulting stress by more than 5 percent.

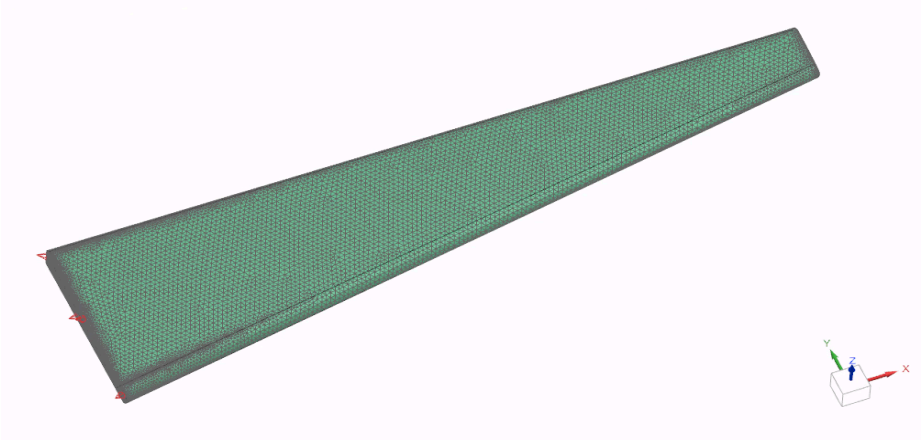

Figure 28: *Tetrahedral mesh of full wing at 4 mm element size.*

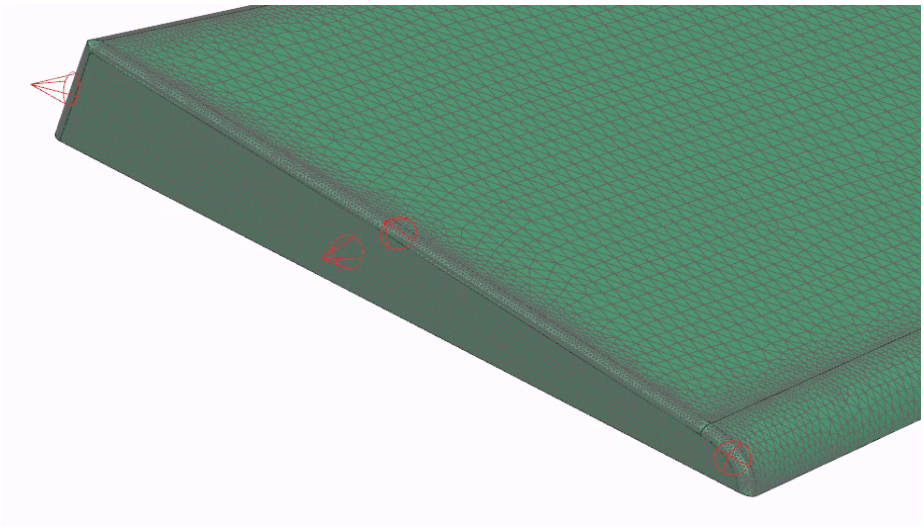

Figure 29: *Mesh refinement down to 1 mm element size at the wing root.*

Material Properties

Three materials were tested: aluminum 6061, ABS plastic, and carbon fiber. Aluminum and ABS were assigned directly using NX library values. The carbon fiber composite was modeled as an equivalent isotropic material to enable direct comparison with aluminum and ABS and to keep the validation against beam theory tractable. While carbon fiber is inherently orthotropic, the loading case here is dominated by in-plane bending, so an equivalent Young's modulus of 75 GPa and a Poisson ratio of 0.25 were used to represent the effective laminate stiffness in this analysis.

Boundary Conditions

The wing root was modeled as a fixed support, constraining all six degrees of freedom to simulate the attachment to the fuselage. This setup is consistent with the cantilever beam assumption used in the analytical validation. With the root fixed, the bending moment is fully transferred to the root and the location of the maximum stress can be predicted directly.

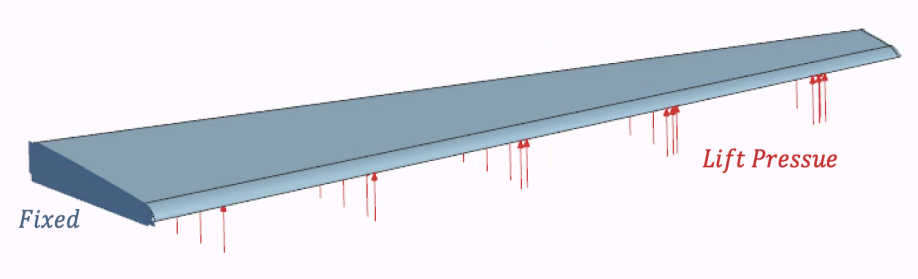

Figure 30: *Boundary and loading conditions of FEA model setup.*

Loading Conditions

Aerodynamic loading was applied as a uniform pressure on the bottom surface of the wing, distributed over its area. The lift force per wing was calculated from a UAV weight of 10 lbf and a load factor n, starting with cruise (n = 1):

$$L_{wing} = (n \cdot W_{UAV}) / 2 = 44.5 / 2 = 22.25\ N$$

The wing area was measured directly from the bottom face of the wing in NX as 0.0576 m². The pressure follows from force divided by area:

$$p = L_{wing} / A_{wing} = 22.25\ N / 0.0576\ m^2 = 386\ Pa$$

This 386 Pa value was used for the cruise loading case. A second case was run at a load factor of n = 4, which corresponds to 1544 Pa, to bracket a high-g maneuver.

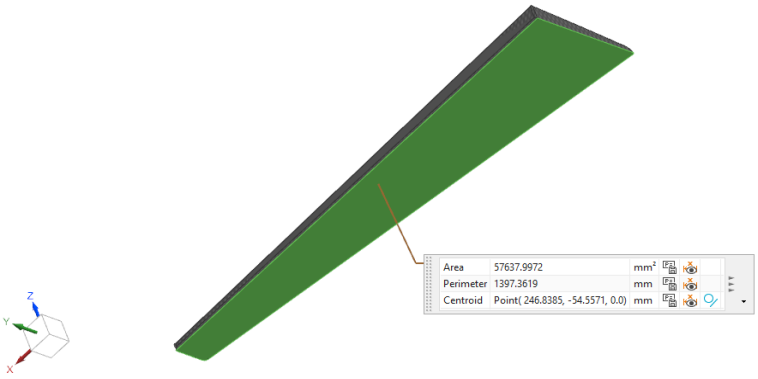

Figure 31: *Wing area calculation in NX, used to back out the cruise pressure.*

Results

The FEA was run for the three materials at the 386 Pa cruise pressure. Maximum stress at the root and maximum tip deflection were extracted.

Table 1: *FEA results for wing response at 386 Pa cruise loading.*

Material	Yield Strength (MPa)	FEA Max Stress, σ (MPa)	FEA Max Deflection, δ (mm)
Carbon Fiber	800 (UTS)	6.510	0.277
Aluminum 6061-T6	240	5.942	0.299
ABS Plastic	40	5.310	10.21

The maximum stress values stayed close across materials at this load. This is consistent with beam bending theory, where stress depends on the moment of inertia and cross section, both of which were held constant. The maximum stress location was the top edge of the root where the wing meets the body, which is also the location predicted by the cantilever model. The maximum stress remained below yield for all three materials with margin to spare. Tip deflection for carbon fiber and aluminum was similar, while ABS was much larger because of the lower stiffness, which is the expected behavior.

Because the cruise stresses were well below yield, a second pass was run at a load factor of n = 4, which gives 1544 Pa. The results for the same three materials are below.

Table 2: *FEA results for wing response at 1544 Pa pull-up loading.*

Material	Yield Strength (MPa)	FEA Max Stress, σ (MPa)	FEA Max Deflection, δ (mm)
Carbon Fiber	800 (UTS)	26.04	1.107
Aluminum 6061-T6	240	23.77	1.195
ABS Plastic	40	21.24	40.92

The stress values scale roughly four times the cruise case, which matches the four-times pressure scaling. Deflection scales the same way, and ABS again separates from the metal and composite. The maximum stress is concentrated at the top of the wing root where it attaches to the body, as shown in Figure 32.

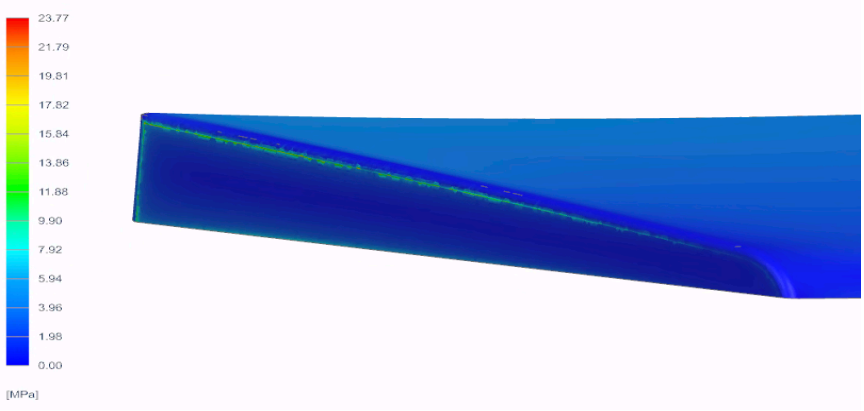

Figure 32: *Maximum wing stress at root under 1544 Pa load (aluminum 6061).*

Maximum deflection occurred at the wing tip, furthest from the root, which matches the cantilever beam expectation.

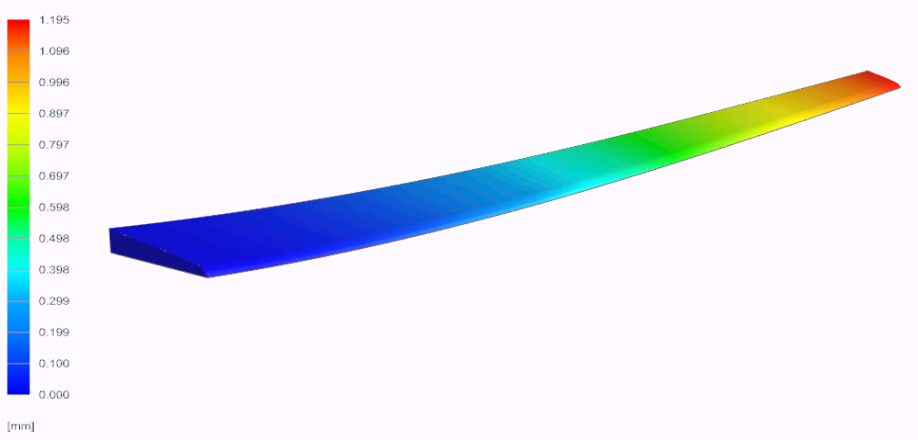

Figure 33: *Maximum wing deflection at tip under 1544 Pa load (aluminum 6061).*

Based on these results, ABS plastic is not suitable for the operating conditions of this UAV. The maximum stress sits at a factor of safety of about 1.88, and the 40 mm tip deflection is roughly 6.2 percent of wing length, which is just outside the 2 to 5 percent range typically used for fixed-wing UAVs. Aluminum 6061 and carbon fiber behave similarly in these isotropic FEA results. Because carbon fiber was modeled as isotropic, a follow-up with a real laminate definition is needed before that material would be locked in.

Landing Gear U-Link

The front landing gear U-link was analyzed for the tension load it sees when the aircraft pulls weight off the wheels during taxi or takeoff rotation. Two outputs were targeted: the nodal stress at the U-bend, which is the location of the highest bending moment in the curved section, and the maximum displacement at the top mount, which sets how much the body fitting deflects under load.

The link was meshed as a 3D tetrahedral solid. AISI 4340 steel was assigned with a yield strength of approximately 470 MPa and a Young's modulus of 200 GPa. The two mounting pins at the bottom of the link were given fixed supports, and a 20 N axial load was applied at the top mount face to represent the

tension transferred from the body fitting. Figures 34 and 35 show the meshed geometry with the load arrow and the simplified loading schematic used to set up the hand calculation.

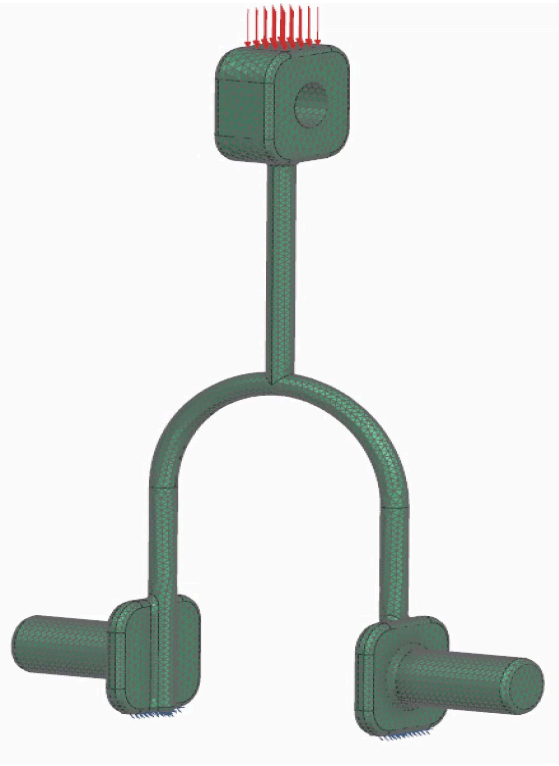

Figure 34: *U-link mesh with applied 20 N tension load at the top mount and fixed pins at the bottom.*

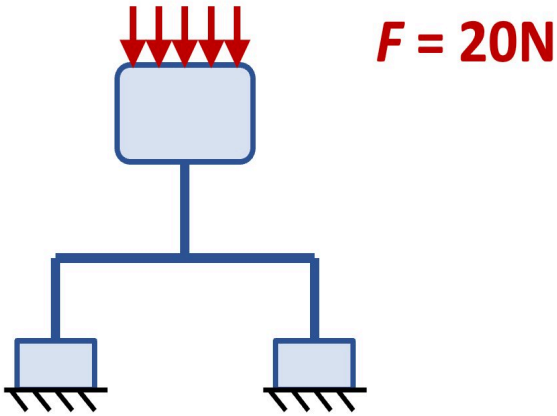

Figure 35: *U-link load schematic showing the 20 N applied force and fixed bottom supports.*

The Von Mises stress contour shows that the highest stress sits in the curved section of the U just above the right pin, where the bending moment is largest. The peak value is 14.65 MPa, well below the 470 MPa yield of AISI 4340. The maximum displacement is 3.231×10^{-3} mm at the top mount, which is the loading point.

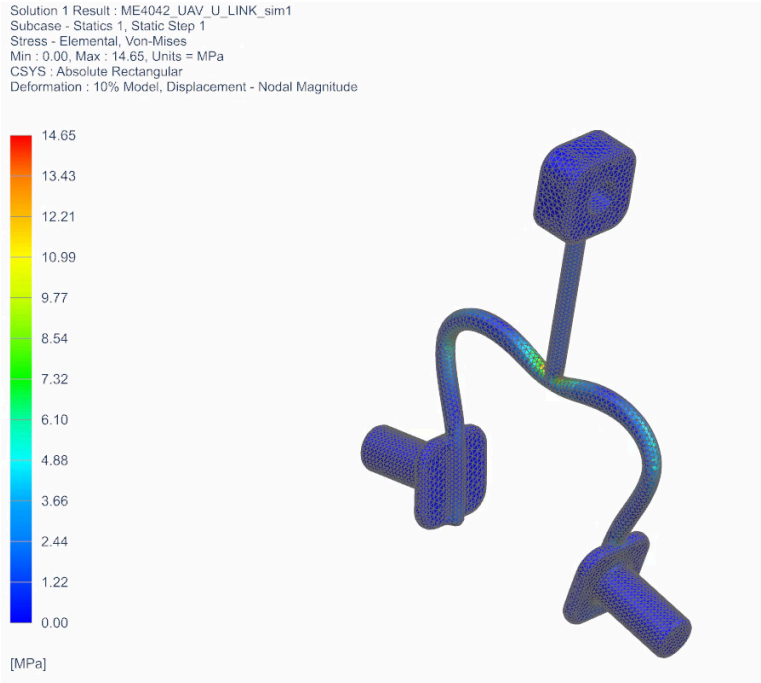

Figure 36: *Von Mises stress on U-link, peaking at 14.65 MPa in the curved section.*

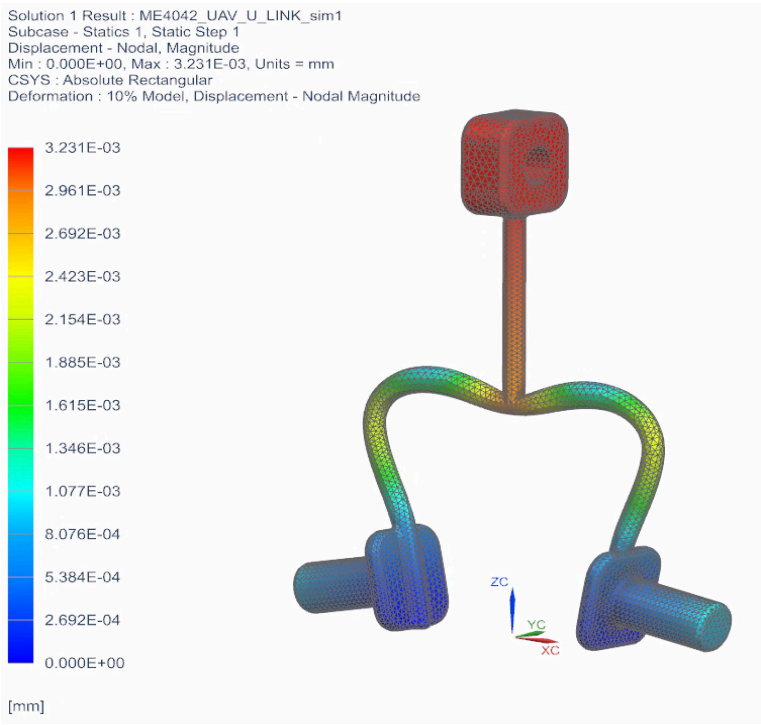

Figure 37: *Nodal displacement on U-link, peaking at 0.003 mm at the top mount.*

At the operational tension load this part is heavily over-designed, with a factor of safety of around 32 against yield. That is acceptable here because AISI 4340 was chosen for the impact case and not the steady-state pull, but it does suggest weight could be removed in a future revision.

Full Assembly Crash Analysis Attempt

A third FEA was set up on the full assembly to look at the load path from a nose impact through the airframe and into the landing gear. The assembly was meshed at component level with a fixed constraint at the front of the fuselage and a forward-pointing force applied at the nose tip to simulate the deceleration into an obstacle. Figure 38 shows the setup with the red force vectors at the nose and the blue fixed-region cylinders at the wheel contact patches.

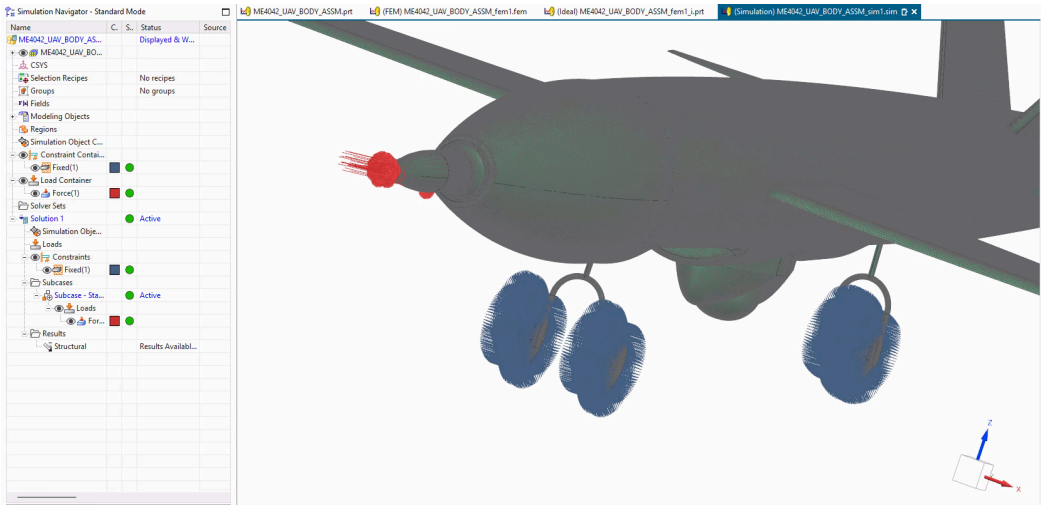

Figure 38: *Full assembly FEA setup for the attempted crash analysis. Force is applied at the nose with the wheels held fixed.*

This run did not converge to a usable result. Even though CTETRA4 was used, the mesh size that worked for an individual wing or U-link was too fine for the full assembly, resulting in a 2.5GB simulation file. The element count grew past what the available memory could carry, and coarsening the mesh enough to fit lost the resolution needed at the nose contact.

What this exercise produced was a clear scoping decision. Component-level FEA on the wing and the U-link is the right level of fidelity for a static analysis with hand-calculation validation. A full crash case belongs in an explicit dynamics solver such as LS-DYNA or Abaqus Explicit, with simplified mass-and-stiffness representations of the non-critical parts and a properly defined contact between the nose and the impacting surface.

FEA Validation

The FEA results were checked against analytical solutions from beam theory. Agreement between the analytical and numerical models gives confidence that the modeling assumptions, boundary conditions, and material properties were applied correctly.

Wings

The wing was approximated as a fixed cantilever beam at the root subjected to a uniformly distributed load along the span. There is no closed-form solution for a pressure load on a tapered beam, so the pressure

was converted to a distributed load using the average chord length, and the wing was treated as a constant-section beam over its 0.6 m span:

$$w = p \cdot c\_avg$$

Average chord length was measured directly in NX as the average of the root and tip widths.

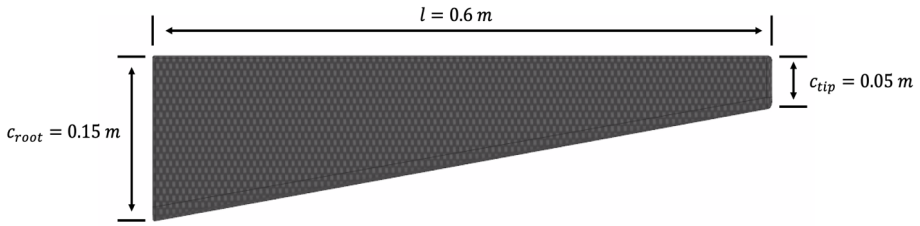

Figure 39: *Average chord length from the side wing geometry.*

$$c\_avg = (c\_root + c\_tip) / 2 = (0.15 + 0.05) / 2 = 0.10\ m$$

$$w = p \cdot c\_avg = 1544\ Pa \cdot 0.10\ m = 154.4\ N/m$$

The 1544 Pa case was used for the validation, with aluminum 6061 as the material. The cantilever beam equations from Shigley's Mechanical Engineering Design were used.

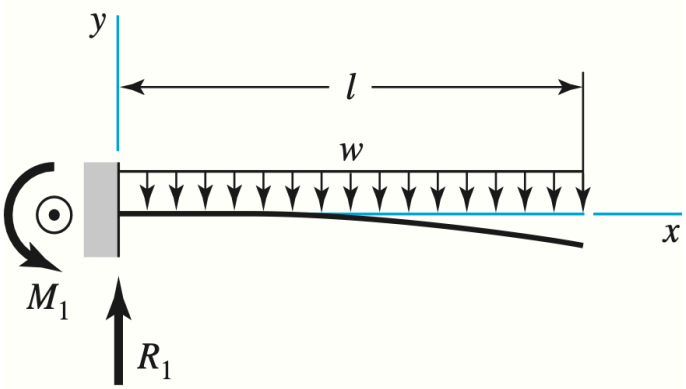

Figure 40: *Distributed load cantilever beam model used for hand calculation.*

$$\delta_{max} = \frac{wl^4}{8EI}$$

$$M_{max} = \frac{wl^2}{2}$$

Figure 41: *Cantilever beam deflection and moment equations used in the validation.*

The moment of inertia of the wing cross section was extracted from the Section Inertia Analysis tool in NX at the root, since the maximum bending moment and the maximum stress both occur there. The minimum-axis MOI was used because that is the axis the wing bends about under lift. The result was 2.64 × 10^4 mm^4.

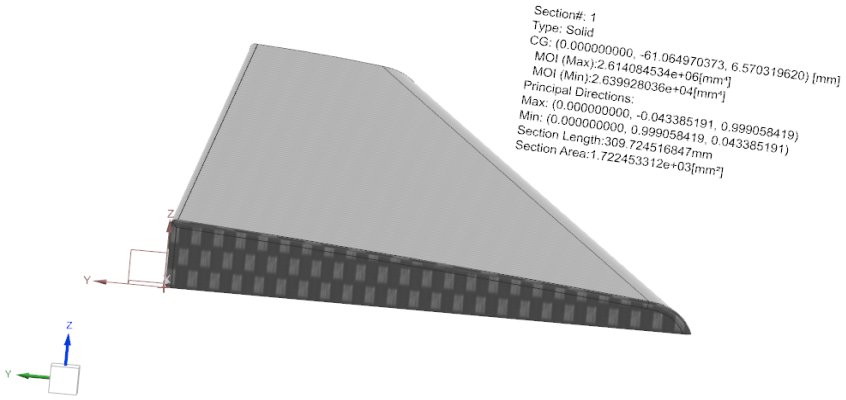

Figure 42: *MOI calculation using the section inertia analysis tool in NX.*

Maximum tip deflection from the analytical model:

$$\delta_{max} = w \cdot l^4 / (8 \cdot E \cdot I) = (154.4)(0.6)^4 / [8 \cdot (6.898 \times 10^{10}) \cdot (2.64 \times 10^{-8})] = 1.37\ mm$$

FEA reported 1.195 mm at the same load and material. The discrepancy is 12.78 percent, which is within the expected range for a tapered airfoil approximated as a constant-section rectangle.

Maximum stress at the root from the analytical model:

$$M_{max} = w \cdot l^2 / 2 = (154.4)(0.6)^2 / 2 = 27.79\ N \cdot m$$

$$\sigma_{max} = M_{max} \cdot c / I = (27.79)(0.01) / (2.64 \times 10^{-8}) = 10.53\ MPa$$

FEA reported 23.77 MPa for aluminum 6061 at 1544 Pa, which is roughly twice the analytical value. The order of magnitude is correct, and the discrepancy is driven by an additional stress concentration at the sharp edge of the airfoil where the trailing edge meets the root. Probing the FEA contour just inboard of that edge gives values in the 11.88 to 13.86 MPa range, which matches the hand calculation closely (Figure 43).

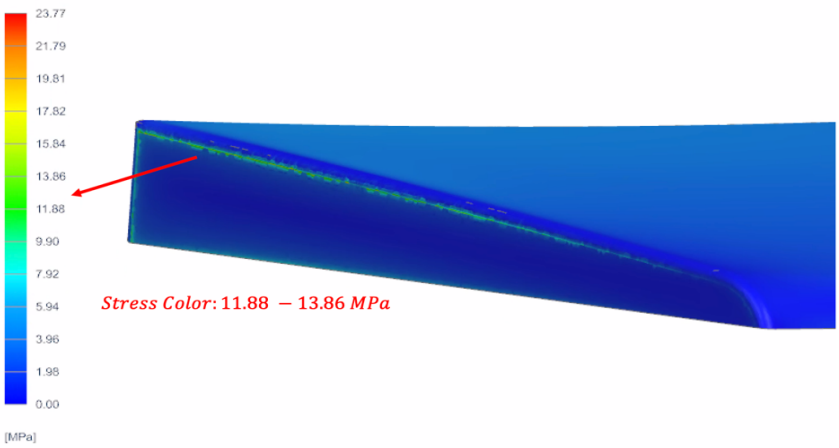

Figure 43: *Stress along the top surface of the wing root falls in the 11.88 to 13.86 MPa range, matching the analytical value once the edge concentration is excluded.*

The deflection match within 13 percent and the stress match within an explainable factor of two support the FEA modeling assumptions and material setup. Further work would refine the carbon fiber model to a real laminate before the wing material is locked in.

Landing Gear U-Link

The U-link was validated as a cantilever bending element. The 20 N axial load applied at the top mount produces a bending moment at the U-bend through the offset between the top mount and the curved section. From the geometry, the moment arm is approximately 40 mm and the local cross section in the bend is a solid circular shaft of about 8 mm diameter.

$$M = F \cdot L = (20)(0.040) = 0.80\ N{\cdot}m$$

Bending stress for a solid circular shaft:

$$\sigma = 32 \cdot M / (\pi \cdot d^3) = 32(0.80) / [\pi(0.008)^3] \approx 15.9\ MPa$$

Cantilever deflection of the loaded section:

$$\delta = F \cdot L^3 / (3 \cdot E \cdot I) \approx 4 \times 10^{-3}\ mm$$

FEA reported a maximum stress of 14.65 MPa and a maximum displacement of 3.23×10^{-3} mm. The stress matches the analytical result within 7.9 percent, and the displacement matches within roughly 25 percent, which is acceptable given that the hand calculation idealizes the curved U-section as a straight cantilever. The factor of safety against yield is:

$$n = \sigma_y / \sigma_{max} = 470 / 14.65 \approx 32$$

That number is high, which is expected for a part that is sized by an impact load case rather than the steady-state tension considered here. The agreement between the FEA and the analytical bending model gives confidence that the U-link FEA is correctly set up and ready for an extension to the impact case.

Future Work

Several extensions to this work are worth pursuing in a follow-up project. Each one is targeted at a specific limitation that this report exposed.

Theoretical landing gear with suspension. The current U-link sees a factor of safety of 32 against the 20 N tension load, which means there is room to add a damping element without exceeding the material limits. A theoretical revision would split the U-link into a sprung upper section and a damped lower section, with a shock absorber between them sized so the steady-state stress climbs from 14.65 MPa to roughly 100 MPa under a 1 m/s touchdown velocity. That brings the factor of safety down to a more reasonable 4 to 5 and gives the airframe a stroke length to absorb the landing impact instead of transmitting it directly into the body. The hand calculation needed for this is a straightforward energy-balance between the kinetic energy at touchdown and the strain energy stored in the spring, and the FEA is a transient dynamics run rather than a static one.

Wings with actuated flaps. The current wings have flaps modeled as separate bodies, but the flaps are static in the assembly. A future revision would drive the flap angle through an assembly variable so the same wing geometry can be analyzed at takeoff (flap deflection of around 20 degrees), cruise (flap neutral), and landing (flap deflection of around 40 degrees). The FEA would need to capture the change in lift distribution and the additional hinge moment at the flap pivot. With the flap as a parameter, the same wing FEA loop can be reused across the three flight regimes without rebuilding the model.

Higher-fidelity carbon fiber. The current FEA uses an isotropic equivalent for the carbon fiber wing. A laminate definition with proper ply orientation would predict different stress and deflection along and across the spanwise fibers, and is the right model before the wing material is locked in for fabrication. The same applies to the propeller blades, which are also carbon fiber in the design intent.

Aerodynamic loading from CFD. The current pressure load is uniform across the bottom of the wing. A CFD run would replace that with a chordwise and spanwise pressure distribution, which would shift the stress and deflection peaks slightly inboard from the root and toward mid-chord. With CFD-driven pressures, the wing geometry could also be iterated for lift-to-drag rather than just structural margin.

Crash analysis in an explicit dynamics solver. The full-assembly crash run that did not converge in static FEA is the natural job for LS-DYNA or Abaqus Explicit. The simplified mass and stiffness model would represent the non-critical parts (rear wings, stabilizers, propeller, payload bay covers) as point masses, while the fuselage, nose, and landing gear would carry full meshes. The output is the deceleration profile at the camera mount, which sets the survivability budget for the sensor payload.

Physical testing. Once the higher-fidelity FEA passes, a static load test on a fabricated wing root and a drop test on the U-link would close the loop on the validation. The instrumentation needed is straightforward: strain gauges at the wing root and an accelerometer on the U-link top mount.

Summary and Conclusion

This project covered the geometric modeling, structural analysis, and validation of a small fixed-wing UAV in Siemens NX. The modeling effort produced a 43-part assembly with surface and solid features, including a hollow-payload fuselage, a wing with a separate flap body, a four-blade propeller, retractable landing gear with hydraulic actuators, and a sensor mount. The FEA effort focused on the wings under distributed lift pressure and the front landing gear U-link under a tension load, and was validated against cantilever beam theory. The wing FEA matched the analytical model on deflection within 13 percent and on stress within an explainable factor that resolved when the local edge concentration was excluded. The U-link FEA matched the analytical bending stress within 8 percent.

A full-assembly crash run was attempted and did not converge. That outcome scoped the future work toward an explicit dynamics solver and a simplified mass-and-stiffness representation of the non-critical parts. Future work was outlined in five directions: a sprung-and-damped landing gear, actuated flaps driven by an assembly variable, a laminate carbon fiber model, CFD-driven aerodynamic loads, and a proper crash analysis in an explicit solver. Together with a static load test on the wing root and a drop test on the U-link, this would close out the design to the point where a flying prototype could be fabricated.

References

[1] R. G. Budynas and J. K. Nisbett, *Shigley's Mechanical Engineering Design*, 11th ed. New York: McGraw-Hill, 2020.

[2] Siemens Digital Industries Software, *NX Documentation: Surface and Solid Modeling, Assemblies, and Simulation*. Plano, TX: Siemens, 2024.

[3] U.S. Air Force Fact Sheet, *MQ-9 Reaper*. Air Combat Command Public Affairs.

[4] Anduril Industries, *ALTIUS-600/700 Product Overview*. Costa Mesa, CA: Anduril.